Universität Karlsruhe (TH)
Institut für Baustatik

A linear quadrilateral shell element with fast stiffness computation

F. Gruttmann, W. Wagner

Mitteilung 1(2004)

Universität Karlsruhe (TH)
Institut für Baustatik

A linear quadrilateral shell element with fast stiffness computation

F. Gruttmann, W. Wagner

Mitteilung 1(2004)

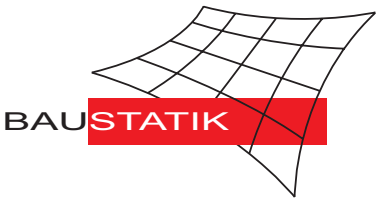

Prof. Dr.–Ing. W. Wagner
Institut für Baustatik
Universität Karlsruhe
Postfach 6980
76128 Karlsruhe

Telefon: (0721) 608–2280
Telefax: (0721) 608–6015
E–mail: bs@.uni-karlsruhe.de
Internet: http://www.bs.uni-karlsruhe.de

A linear quadrilateral shell element with fast stiffness computation

F. Gruttmann
Institut für Werkstof
und Mechanik im Bauwesen
Technische Universität Darmstadt
Petersenstraße 12
64287 Darmstadt
Germany

W. Wagner
Institut für Baustatik
Universität Karlsruhe (TH)
Kaiserstraße 12
76131 Karlsruhe
Germany

Contents

Abstract

A new quadrilateral shell element with 5/6 nodal degrees of freedom is presented. Assuming linear isotropic elasticity a Hellinger–Reissner functional with independent displacements, rotations and stress resultants is used. Within the mixed formulation the stress resultants are interpolated using five parameters for the membrane forces as well as for the bending moments and four parameters for the shear forces. The hybrid element stiffness matrix resulting from the stationary condition is integrated analytically. This leads to a part obtained by one point integration and a stabilization matrix. The element possesses the correct rank, is free of locking and is applicable within the whole range of thin and thick shells. The in–plane and bending patch tests are fulfilled and the computed numerical examples show that the convergence behaviour of the stress resultants is very good in comparison to comparable existing elements. The essential advantage is the fast stiffness computation due to the analytically integrated matrices.

Keywords Reissner–Mindlin shell theory, Hellinger–Reissner variational principle, quadrilateral shell element, effective analytical stiffness evaluation, one point integration and stabilization matrix, in–plane and bending patch test

1 Introduction

Computational shell analysis is based on stress resultant theories e.g. [1, 2] or on the so–called degenerated approach [3]. New developments in this field are discussed in e.g. [4, 5]. In the following only the main computational aspects are considered. Although the hypothesis underlying the degenerated approach and classical shell theory are essentially the same, the reduction to resultant form is typically carried out numerically in the former, and analytically in the latter, [6]. Many of the computational shell models consider transverse shear deformations within a Reissner–Mindlin theory [7], [8] to by–pass the difficulties caused by C^1–requirements of the Kirchhoff–Love theory, see e.g. [9, 10, 11].

Generally, shell behaviour is extremely sensitive to initial geometry and imperfections, thus a successful correlation between theory and analysis is achieved only after including specific details of these quantities. Low order elements like quadrilaterals based on standard displacement interpolation are usually characterized by locking phenomena. In shells two types of locking occur: transverse shear locking in which bending modes are excluded and nearly all energy is stored in transverse shear terms, and; membrane locking in which all bending energy is restrained and energy is stored in membrane terms. Elements which exhibit a locking tendency lead to unacceptable stiff results when reasonable finite element meshes are employed.

In attempting to avoid locking, reduced integration methods have often been advocated, see e.g. [12]. Use of reduced (or selective reduced) integration is often accompanied by spurious zero energy modes. Hence, authors have developed stabilization techniques to regain the correct rank of the element stiffness matrix, e.g. [13, 14, 9]. In some cases, however, results computed using these formulations turned out to be sensitive to the ad hoc hourglass control parameters. Furthermore these elements do not fulfill the bending patch test.

An effective method to avoid transverse shear locking is based on assumed shear strain fields first proposed in [15], and subsequently extended and reformulated in [16, 17, 18, 19].

Mixed variational principles provide the basis for the discussed finite element techniques. Assuming linear elasticity a Hellinger–Reissner functional has been used in e.g. [20, 21]. Ref. [20] describe a quadrilateral element with assumed stresses for membrane, bending and shear parts whereas in Ref [21] explicit stabilization matrices for a nine node element have been derived. For general nonlinear material behaviour a three field variational functional with independent displacements, stresses and strains is more appropriate. Within the so–called enhanced strain formulations the independent stresses are eliminated from the set of equations using orthogonality conditions and a two field formulation remains, [22]. For shells this method has been applied enhancing the Green–Lagrangean membrane strains e.g. in [23].

The drawbacks in [13, 14, 9] have been overcome in [24]. The theory is based on a Hu–Washizu three–field variational principle with independent displacements, stresses and strains. The stabilization matrix is derived from the orthogonality between the constant part of the strain field and the non-constant part using 5 degrees of freedom at each node. In this context we also refer to [25] where an updated Lagrangian approach is used. Further developments for different boundary value problems are considered in [26], where stabilization matrices on basis of the enhanced strain method have been derived.

An important issue within the context of developing a finite shell model is the number and type of rotational parameters on the element. Mostly general shell theories exclude explicit dependence of a rotational field about the normal to the shell surface which leads to a five parameter model (three displacements and two local rotations). Use of 5 degree–of–freedom frame requires construction of special coordinate systems for the rotational parameters. Considering the so–called drilling degree-of–freedom leads to a finite element discretization with six nodal parameters. This has some advantages since both displacement and rotation parameters are associated with a global coordinate frame. On the other hand a larger set of algebraic equations has to be solved. In this context we mention the four–node shell element according to [27] with three global displacements and three global rotations at each node. The element employs a membrane interpolation field with drilling degrees–of–freedom. The bending stiffness is based on the discrete Kirchhoff theory. For arbitrary shaped elements a transformation of the stiffness matrix, which considers the warping effects, leads to good results also for a non–flat geometry. The element [27] has been widely used in the literature for comparisons, e.g. in [10] and in the present paper.

The essential features and new contributions of the present formulation are summarized as follows:

(i) Assuming linear elasticity the variational formulation of the shear–elastic shell is based on the Hellinger–Reissner principle. We specify the shape functions for the independent stress resultants, where the interpolation of the membrane forces and of the bending moments corresponds to the approach in [10]. Here, the new contribution is the analytical integration of the matrices, which leads to a one–point integrated part and an explicit stabilization matrix. This requires the replacement of the variable base vectors and director vectors by those of the element center, which corresponds to a projection on a flat surface, see also [27]. For warped elements the above mentioned transformation according to [27] is implemented.

(ii) The interpolation of the shear forces along with assumed shear strains and the explicit matrix representation of the stabilization matrix is a further new contribution.

(iii) The element possesses with six zero eigenvalues the correct rank. No control parameters have to be chosen to prevent locking or to avoid hour–glassing. The in–plane and bending patch tests are fulfilled. Especially the convergence behaviour of the stress resultants is superior to comparable four–node shell elements. The main advantage is the fast stiffness computation. In our implementation the present formulation requires only about 60% of the computing time to setup the global stiffness matrix compared with the element [27].

(iv) The element formulation allows the analysis of shells with intersections. At all nodes which are not positioned on intersections the drilling degree of freedom is fixed. Thus, the nodal degrees of freedom are: three global displacements components, three global rotations at nodes on intersections and two local rotations at other nodes.

2 Kinematics and Variational Formulation

Let $\mathcal{B}_0$ be the three–dimensional Euclidean space occupied by the shell in the un–deformed configuration with boundary $\partial\mathcal{B}_0$. The position vector $\mathbf{\Phi}$ of any point $P \in \mathcal{B}_0$ is associated with the global coordinate frame $\mathbf{e}_i$

$$\begin{aligned} &\mathbf{\Phi}(\xi^1,\xi^2,\xi^3) = \Phi^i\,\mathbf{e}_i = \mathbf{X} + \xi^3\,\mathbf{D}(\xi^1,\xi^2) \\ &\text{with} \quad |\mathbf{D}(\xi^1,\xi^2)| = 1 \quad \text{and} \quad -\frac{h}{2} \le \xi^3 \le \frac{h}{2} \end{aligned} \tag{1}$$

with the position vector $\mathbf{X}(\xi^1,\xi^2)$ of the shell mid–surface Ω, the shell thickness h, and ξ^i the convected coordinate system of the body. A director $\mathbf{D}(\xi^1,\xi^2)$ is defined as a vector perpendicular to the shell mid–surface. The usual summation convention is used, where Latin indices range from 1 to 3 and Greek indices range from 1 to 2. Commas denote partial differentiation with respect to the coordinates ξ^i.

Hence, the geometry of the deformed shell space $\mathcal{B}$ is described by

$$\boldsymbol{\phi}(\xi^1,\xi^2,\xi^3) = \phi^i\,\mathbf{e}_i = \mathbf{x}(\xi^1,\xi^2) + \xi^3\,\mathbf{d}(\xi^1,\xi^2) \quad \text{with} \quad \mathbf{d} = \mathbf{D} + \Delta\mathbf{d}\,. \tag{2}$$

With the kinematic assumption (2) shear deformations are accounted for and thus $\mathbf{d}$ is not normal to the deformed shell mid–surface.

Inserting the position vectors (1) and (2) in the linear strain tensor $\bar{\boldsymbol{\varepsilon}}$ one obtains

$$\bar{\boldsymbol{\varepsilon}} = \bar{\varepsilon}_{ij}\,\mathbf{G}^i \otimes \mathbf{G}^j \qquad \bar{\varepsilon}_{\alpha\beta} = \varepsilon_{\alpha\beta} + \xi^3\,\kappa_{\alpha\beta} \qquad 2\,\bar{\varepsilon}_{\alpha 3} = \gamma_\alpha \qquad \bar{\varepsilon}_{33} = 0\,, \tag{3}$$

where $\mathbf{G}^i$ denote the contravariant base vectors. The membrane strains $\varepsilon_{\alpha\beta}$, curvatures $\kappa_{\alpha\beta}$ and shear strains γ_α read

$$\begin{aligned} \varepsilon_{\alpha\beta} &= \frac{1}{2}(\mathbf{u}_{,\alpha}\cdot\mathbf{X}_{,\beta} + \mathbf{u}_{,\beta}\cdot\mathbf{X}_{,\alpha}) \\ \kappa_{\alpha\beta} &= \frac{1}{2}(\mathbf{u}_{,\alpha}\cdot\mathbf{D}_{,\beta} + \mathbf{u}_{,\beta}\cdot\mathbf{D}_{,\alpha} + \mathbf{X}_{,\alpha}\cdot\Delta\mathbf{d}_{,\beta} + \mathbf{X}_{,\beta}\cdot\Delta\mathbf{d}_{,\alpha}) \\ \gamma_\alpha &= \mathbf{u}_{,\alpha}\cdot\mathbf{D} + \mathbf{X}_{,\alpha}\cdot\Delta\mathbf{d}\,. \end{aligned} \tag{4}$$

and are organized in a vector $\boldsymbol{\varepsilon} = [\varepsilon_{11}, \varepsilon_{22}, 2\varepsilon_{12}, \kappa_{11}, \kappa_{22}, 2\kappa_{12}, \gamma_1, \gamma_2]^T$.

The variational formulation is based on a Hellinger–Reissner functional, where the displacement field and the stress resultants are independent. The shell is loaded by loads $\bar{\mathbf{p}}$ in Ω and by boundary loads $\bar{\mathbf{t}}$ on a part of the boundary Γ_σ. The potential is a function of the displacement field $\mathbf{v} = [\mathbf{u}, \Delta\mathbf{d}]^T$ with $\mathbf{u} = \mathbf{x} - \mathbf{X}$ and the stress resultants $\boldsymbol{\sigma} = [n_{11}, n_{22}, n_{12}, m_{11}, m_{22}, m_{12}, q_1, q_2]^T$ with membrane forces $n_{\alpha\beta}$, bending moments $m_{\alpha\beta}$ and shear forces q_α

$$\Pi_{HR}(\mathbf{v}, \boldsymbol{\sigma}) = \int\limits_{(\Omega)} (\boldsymbol{\varepsilon}^T \boldsymbol{\sigma} - \frac{1}{2}\boldsymbol{\sigma}^T \mathbf{C}^{-1} \boldsymbol{\sigma})\, dA - \int\limits_{(\Omega)} \mathbf{u}^T \bar{\mathbf{p}}\, dA - \int\limits_{(\Gamma_\sigma)} \mathbf{u}^T \bar{\mathbf{t}}\, ds \;\rightarrow\; \text{stat.} \tag{5}$$

Assuming linear isotropic elasticity the constitutive matrix reads

$$\mathbf{C} = \begin{bmatrix} \mathbf{C}^m & \mathbf{0} & \mathbf{0} \\ \mathbf{0} & \mathbf{C}^b & \mathbf{0} \\ \mathbf{0} & \mathbf{0} & \mathbf{C}^s \end{bmatrix} \quad \text{with} \quad \boldsymbol{C}^m = \frac{Eh}{1-\nu^2} \begin{bmatrix} 1 & \nu & 0 \\ \nu & 1 & 0 \\ 0 & 0 & \dfrac{1-\nu}{2} \end{bmatrix}, \quad \begin{aligned} \mathbf{C}^b &= \frac{h^2}{12}\boldsymbol{C}^m \\ \mathbf{C}^s &= \kappa G h\, \mathbf{1}_2 \end{aligned}, \tag{6}$$

with the second order unit matrix $\mathbf{1}_2$, Young´s modulus E, shear modulus G, Poisson´s ratio ν and shear correction factor $\kappa = \frac{5}{6}$.

The stationary condition yields

$$\delta\Pi_{HR}(\mathbf{v}, \boldsymbol{\sigma}, \delta\mathbf{v}, \delta\boldsymbol{\sigma}) = \int\limits_{(\Omega)} [\delta\boldsymbol{\varepsilon}^T\, \boldsymbol{\sigma} + \delta\boldsymbol{\sigma}^T\, (\boldsymbol{\varepsilon} - \mathbf{C}^{-1}\boldsymbol{\sigma}) - \delta\mathbf{u}^T \bar{\mathbf{p}}]\, dA - \int\limits_{(\Gamma_\sigma)} \delta\mathbf{u}^T\, \bar{\mathbf{t}}\, ds = 0 \tag{7}$$

with virtual displacements $\delta\mathbf{v} = [\delta\mathbf{u}, \delta\mathbf{d}]^T$ and virtual stress resultants $\delta\boldsymbol{\sigma} = [\delta n_{11}, \delta n_{22}, \delta n_{12}, \delta m_{11}, \delta m_{22}, \delta m_{12}, \delta q_1, \delta q_2]^T$. The virtual shell strains read

$$\begin{aligned} \delta\varepsilon_{\alpha\beta} &= \frac{1}{2}(\delta\mathbf{u}_{,\alpha} \cdot \mathbf{X}_{,\beta} + \delta\mathbf{u}_{,\beta} \cdot \mathbf{X}_{,\alpha}) \\ \delta\kappa_{\alpha\beta} &= \frac{1}{2}(\delta\mathbf{u}_{,\alpha} \cdot \mathbf{D}_{,\beta} + \delta\mathbf{u}_{,\beta} \cdot \mathbf{D}_{,\alpha} + \mathbf{X}_{,\alpha} \cdot \delta\mathbf{d}_{,\beta} + \mathbf{X}_{,\beta} \cdot \delta\mathbf{d}_{,\alpha}) \\ \delta\gamma_\alpha &= \delta\mathbf{u}_{,\alpha} \cdot \mathbf{D} + \mathbf{X}_{,\alpha} \cdot \delta\mathbf{d} \end{aligned} \tag{8}$$

and are summarized in vector notation $\delta\boldsymbol{\varepsilon} = [\delta\varepsilon_{11}, \delta\varepsilon_{22}, 2\delta\varepsilon_{12}, \delta\kappa_{11}, \delta\kappa_{22}, 2\delta\kappa_{12}, \delta\gamma_1, \delta\gamma_2]^T$.

3 Finite Element Equations

3.1 Mid–Surface and Displacement Interpolation

For a quadrilateral element we exploit the isoparametric concept with coordinates ξ and η defined in the unit square $\{\xi, \eta\} \in [-1, 1]$. Hence the position vector and the director vector of the shell mid–surface are interpolated using the bi–linear functions

$$\begin{aligned} &N_I = \tfrac{1}{4}(1 + \xi_I\xi)(1 + \eta_I\eta) = a_{0I} + a_{1I}\,\xi + a_{2I}\,\eta + h_I\,\xi\eta \\ &\xi_I \in \{-1, \quad 1, \quad 1, -1\} \qquad\qquad \eta_I \in \{-1, -1, \quad 1, \quad 1\} \\ &a_{0I} = \tfrac{1}{4} \qquad a_{1I} = \tfrac{1}{4}\,\xi_I \qquad a_{2I} = \tfrac{1}{4}\,\eta_I \qquad h_I = \tfrac{1}{4}\,\xi_I\,\eta_I \end{aligned} \tag{9}$$

as follows

$$\mathbf{X}^h = \sum_{I=1}^{4} N_I \mathbf{X}_I \qquad\qquad \mathbf{D}^h = \sum_{I=1}^{4} N_I \mathbf{D}_I \,, \tag{10}$$

where the index h denotes the finite element approximation. The position vectors $\mathbf{X}_I$ and the local cartesian basis systems $\mathbf{a}_{kI},\ k = 1, 2, 3$ are generated within the mesh input. Here, $\mathbf{D}_I = \mathbf{a}_{3I}$ is perpendicular to Ω and $\mathbf{a}_{1I}$, $\mathbf{a}_{2I}$ are constructed in such a way that the boundary conditions can be accommodated. With $(10)_2$ the orthogonality is only given at the nodes.

Furthermore, a local cartesian basis $\mathbf{t}_i$ is introduced at the element center

$$\begin{aligned} \bar{\mathbf{d}}_1 &= \mathbf{X}_3 - \mathbf{X}_1 & \mathbf{d}_1 &= \bar{\mathbf{d}}_1/|\bar{\mathbf{d}}_1| \\ \bar{\mathbf{d}}_2 &= \mathbf{X}_2 - \mathbf{X}_4 & \mathbf{d}_2 &= \bar{\mathbf{d}}_2/|\bar{\mathbf{d}}_2| \\ \\ \mathbf{t}_1 &= (\mathbf{d}_1 + \mathbf{d}_2)/|\mathbf{d}_1 + \mathbf{d}_2| \\ \mathbf{t}_2 &= (\mathbf{d}_1 - \mathbf{d}_2)/|\mathbf{d}_1 - \mathbf{d}_2| \\ \mathbf{t}_3 &= \mathbf{t}_1 \times \mathbf{t}_2 \end{aligned} \tag{11}$$

The shell mid–surface described by $(10)_1$ is in general a non–planar surface Ω^h, whereas the flat projection introduced by $\mathbf{t}_1$ and $\mathbf{t}_2$ is denoted by Ω_0^h, see Fig. 1 and Ref. [27].

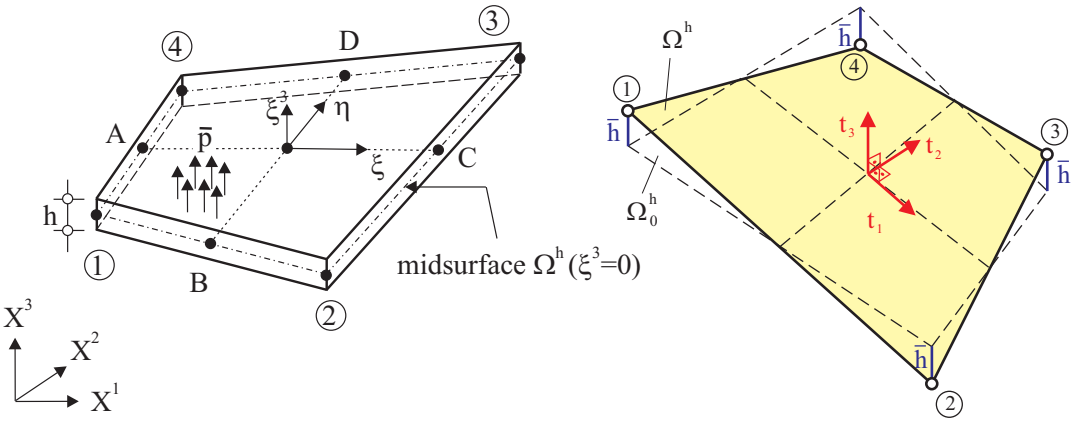

Figure 1: Quadrilateral shell element

The displacements and rotations are interpolated using also the bi–linear functions

$$\mathbf{u}^h = \sum_{I=1}^{4} N_I \mathbf{u}_I \qquad\qquad \Delta\mathbf{d}^h = \sum_{I=1}^{4} N_I \Delta\mathbf{d}_I \,. \tag{12}$$

Here, $\mathbf{u}_I = u_{Ik}\,\mathbf{e}_k$ describes the nodal displacement vector and $\Delta\mathbf{d}_I = \boldsymbol{\varphi}_I \times \mathbf{D}_I$ is given with the nodal rotation vector $\boldsymbol{\varphi}_I = \varphi_{Ik}\,\mathbf{e}_k$ where φ_{Ik} are rotations about global cartesian axes. The virtual displacements $\delta\mathbf{u}$ and rotations $\delta\mathbf{d}$ are approximated in the same way.

3.2 Transverse Shear Strains

The fulfillment of the bending patch test is discussed in [28], where for a plate it is shown, that with the transverse shear strains $(4)_3$ the patch test can not be fulfilled within the

present mixed formulation. The non constant part of the shear strains according to $(4)_3$ leads for a constant stress state to a contribution of the shear energy on the element level.

For this reason we approximate the shear strains with independent interpolation functions proposed in [18, 19] as follows

$$\begin{bmatrix} \gamma_1 \\ \gamma_2 \end{bmatrix} = \mathbf{J}^{-1} \begin{bmatrix} \gamma_\xi \\ \gamma_\eta \end{bmatrix} \quad \text{where} \quad \begin{aligned} \gamma_\xi &= \frac{1}{2}[(1-\eta)\gamma_\xi^B + (1+\eta)\gamma_\xi^D] \\ \gamma_\eta &= \frac{1}{2}[(1-\xi)\gamma_\eta^A + (1+\xi)\gamma_\eta^C] \end{aligned} \tag{13}$$

The strains at the midside nodes A, B, C, D according to Fig. 1 are specified as follows

$$\begin{aligned} \gamma_\xi^M &= [\mathbf{u}_{,\xi} \cdot \mathbf{D} + \mathbf{X}_{,\xi} \cdot \Delta\mathbf{d}]^M \qquad M = B, D \\ \gamma_\eta^L &= [\mathbf{u}_{,\eta} \cdot \mathbf{D} + \mathbf{X}_{,\eta} \cdot \Delta\mathbf{d}]^L \qquad L = A, C \end{aligned} \tag{14}$$

where the following quantities are given with the bilinear interpolation (10)

$$\begin{aligned} \mathbf{D}^A &= \tfrac{1}{2}(\mathbf{D}_4 + \mathbf{D}_1) & \Delta\mathbf{d}^A &= \tfrac{1}{2}(\Delta\mathbf{d}_4 + \Delta\mathbf{d}_1) \\ \mathbf{D}^B &= \tfrac{1}{2}(\mathbf{D}_1 + \mathbf{D}_2) & \Delta\mathbf{d}^B &= \tfrac{1}{2}(\Delta\mathbf{d}_1 + \Delta\mathbf{d}_2) \\ \mathbf{D}^C &= \tfrac{1}{2}(\mathbf{D}_2 + \mathbf{D}_3) & \Delta\mathbf{d}^C &= \tfrac{1}{2}(\Delta\mathbf{d}_2 + \Delta\mathbf{d}_3) \\ \mathbf{D}^D &= \tfrac{1}{2}(\mathbf{D}_3 + \mathbf{D}_4) & \Delta\mathbf{d}^D &= \tfrac{1}{2}(\Delta\mathbf{d}_3 + \Delta\mathbf{d}_4) \\ \mathbf{X}_{,\eta}^A &= \tfrac{1}{2}(\mathbf{X}_4 - \mathbf{X}_1) & \mathbf{u}_{,\eta}^A &= \tfrac{1}{2}(\mathbf{u}_4 - \mathbf{u}_1) \\ \mathbf{X}_{,\xi}^B &= \tfrac{1}{2}(\mathbf{X}_2 - \mathbf{X}_1) & \mathbf{u}_{,\xi}^B &= \tfrac{1}{2}(\mathbf{u}_2 - \mathbf{u}_1) \\ \mathbf{X}_{,\eta}^C &= \tfrac{1}{2}(\mathbf{X}_3 - \mathbf{X}_2) & \mathbf{u}_{,\eta}^C &= \tfrac{1}{2}(\mathbf{u}_3 - \mathbf{u}_2) \\ \mathbf{X}_{,\xi}^D &= \tfrac{1}{2}(\mathbf{X}_3 - \mathbf{X}_4) & \mathbf{u}_{,\xi}^D &= \tfrac{1}{2}(\mathbf{u}_3 - \mathbf{u}_4) \end{aligned} \tag{15}$$

Remark:
An alternative three field variational formulation based on a Hu–Washizu principle for the shear part, which would be the appropriate variational formulation for an independent shear interpolation, leads to identical finite element matrices due to the fact that the shear stiffness matrix is diagonal.

3.3 Discrete Strain Displacement Matrix

Considering (4) and the finite element equations (10) - (15) the approximation of the strains is now obtained by

$$\boldsymbol{\varepsilon}^h = \sum_{I=1}^{4} \mathbf{B}_I \, \mathbf{v}_I \,, \qquad \mathbf{v}_I = [\mathbf{u}_I, \boldsymbol{\varphi}_I]^T \,, \tag{16}$$

with

$$\mathbf{B}_I = \begin{bmatrix} N_{I,1}\,\mathbf{X}_{,1}^T & \mathbf{0} \\ N_{I,2}\,\mathbf{X}_{,2}^T & \mathbf{0} \\ N_{I,1}\,\mathbf{X}_{,2}^T + N_{I,2}\,\mathbf{X}_{,1}^T & \mathbf{0} \\ N_{I,1}\,\mathbf{D}_{,1}^T & N_{I,1}\,\mathbf{b}_{1I}^T \\ N_{I,2}\,\mathbf{D}_{,2}^T & N_{I,2}\,\mathbf{b}_{2I}^T \\ N_{I,1}\,\mathbf{D}_{,2}^T + N_{I,2}\,\mathbf{D}_{,1}^T & N_{I,1}\,\mathbf{b}_{2I}^T + N_{I,2}\,\mathbf{b}_{1I}^T \\ \mathbf{J}^{-1} \begin{Bmatrix} N_{I,\xi}\,\mathbf{D}_M^T \\ N_{I,\eta}\,\mathbf{D}_L^T \end{Bmatrix} & \mathbf{J}^{-1} \begin{Bmatrix} N_{I,\xi}\,\xi_I\,\mathbf{b}_M^T \\ N_{I,\eta}\,\eta_I\,\mathbf{b}_L^T \end{Bmatrix} \end{bmatrix} \tag{17}$$

and $\mathbf{b}_{\alpha I} = \mathbf{D}_I \times \mathbf{X}_{,\alpha} = \mathbf{W}_I\,\mathbf{X}_{,\alpha}$, $\mathbf{b}_M = \mathbf{W}_I\,\mathbf{X}_{,\xi}^M$, $\mathbf{b}_L = \mathbf{W}_I\,\mathbf{X}_{,\eta}^L$. The allocation of the mid–side nodes to the corner nodes is given by $(I, M, L) \in \{(1, B, A); (2, B, C); (3, D, C); (4, D, A)\}$. The skew–symmetric matrix $\mathbf{W}_I$ is associated to $\mathbf{D}_I = D_{Ik}\,\mathbf{e}_k$ as follows

$$\mathbf{W}_I = \operatorname{skew} \mathbf{D}_I = \begin{bmatrix} 0 & -D_{I3} & D_{I2} \\ D_{I3} & 0 & -D_{I1} \\ -D_{I2} & D_{I1} & 0 \end{bmatrix}. \tag{18}$$

Furthermore, the derivatives of the position vectors $\mathbf{X}_{,\alpha}$ and director vectors $\mathbf{D}_{,\alpha}$ are obtained from (10) in a standard way using

$$\begin{bmatrix} N_{I,1} \\ N_{I,1} \end{bmatrix} = \mathbf{J}^{-1} \begin{bmatrix} N_{I,\xi} \\ N_{I,\eta} \end{bmatrix} \qquad \mathbf{J} = \begin{bmatrix} x^L{}_{,\xi} & y^L{}_{,\xi} \\ x^L{}_{,\eta} & y^L{}_{,\eta} \end{bmatrix} = \begin{bmatrix} \mathbf{G}_\xi \cdot \mathbf{t}_1 & \mathbf{G}_\xi \cdot \mathbf{t}_2 \\ \mathbf{G}_\eta \cdot \mathbf{t}_1 & \mathbf{G}_\eta \cdot \mathbf{t}_2 \end{bmatrix}. \tag{19}$$

Here, $\mathbf{J}$ denotes the Jacobian matrix where the local coordinates $x^L = (\mathbf{X} - \mathbf{X}_0) \cdot \mathbf{t}_1$ and $y^L = (\mathbf{X} - \mathbf{X}_0) \cdot \mathbf{t}_2$ are computed with the position vector of the element center $\mathbf{X}_0$. The base vectors are obtained from

$$\begin{aligned} \mathbf{G}_\xi &= \mathbf{G}_\xi^0 + \eta\,\mathbf{G}^1 & \mathbf{G}_\xi^0 &= \sum_{I=1}^4 a_{1I}\,\mathbf{X}_I \\ \mathbf{G}_\eta &= \mathbf{G}_\eta^0 + \xi\,\mathbf{G}^1 & \mathbf{G}_\eta^0 &= \sum_{I=1}^4 a_{2I}\,\mathbf{X}_I \\ & & \mathbf{G}^1 &= \sum_{I=1}^4 h_I\,\mathbf{X}_I\,. \end{aligned} \tag{20}$$

The determinant of $\mathbf{J}$ yields

$$\begin{aligned} \det \mathbf{J} &= j_0 + \xi\,j_1 + \eta\,j_2 \\ j_0 &= (\mathbf{G}_\xi^0 \cdot \mathbf{t}_1)(\mathbf{G}_\eta^0 \cdot \mathbf{t}_2) - (\mathbf{G}_\eta^0 \cdot \mathbf{t}_1)(\mathbf{G}_\xi^0 \cdot \mathbf{t}_2) \\ j_1 &= (\mathbf{G}_\xi^0 \cdot \mathbf{t}_1)(\mathbf{G}^1 \cdot \mathbf{t}_2) - (\mathbf{G}^1 \cdot \mathbf{t}_1)(\mathbf{G}_\xi^0 \cdot \mathbf{t}_2) \\ j_2 &= (\mathbf{G}^1 \cdot \mathbf{t}_1)(\mathbf{G}_\eta^0 \cdot \mathbf{t}_2) - (\mathbf{G}_\eta^0 \cdot \mathbf{t}_1)(\mathbf{G}^1 \cdot \mathbf{t}_2)\,. \end{aligned} \tag{21}$$

Note, that $z^L = (\mathbf{X} - \mathbf{X}_0) \cdot \mathbf{t}_3$ does not enter in (19), which makes clear that the below computed matrices are defined in Ω_0^h.

3.4 Interpolation of the Stress Resultants

The independent field of stress resultants $\boldsymbol{\sigma}$ is interpolated as follows

$$
\begin{aligned}
\boldsymbol{\sigma}^h &= \mathbf{S}\,\boldsymbol{\beta} \\
\mathbf{S} &= \begin{bmatrix} \mathbf{1}_3 & \mathbf{0} & \mathbf{0} & \mathbf{S}^m & \mathbf{0} & \mathbf{0} \\ \mathbf{0} & \mathbf{1}_3 & \mathbf{0} & \mathbf{0} & \mathbf{S}^b & \mathbf{0} \\ \mathbf{0} & \mathbf{0} & \mathbf{1}_2 & \mathbf{0} & \mathbf{0} & \mathbf{S}^s \end{bmatrix} \\
\mathbf{S}^m = \mathbf{S}^b &= \begin{bmatrix} J_{11}^0 J_{11}^0(\eta-\bar{\eta}) & J_{21}^0 J_{21}^0(\xi-\bar{\xi}) \\ J_{12}^0 J_{12}^0(\eta-\bar{\eta}) & J_{22}^0 J_{22}^0(\xi-\bar{\xi}) \\ J_{11}^0 J_{12}^0(\eta-\bar{\eta}) & J_{21}^0 J_{22}^0(\xi-\bar{\xi}) \end{bmatrix} \\
\mathbf{S}^s &= \begin{bmatrix} J_{11}^0(\eta-\bar{\eta}) & J_{21}^0(\xi-\bar{\xi}) \\ J_{12}^0(\eta-\bar{\eta}) & J_{22}^0(\xi-\bar{\xi}) \end{bmatrix}.
\end{aligned}
\tag{22}
$$

Here, we denote by $\mathbf{1}_2, \mathbf{1}_3$ second and third order unit matrices, respectively. The vector $\boldsymbol{\beta}$ contains 8 parameters for the constant part and 6 parameters for the varying part of the stress field, respectively. The interpolation of the membrane forces and the bending moments in (22) corresponds to the procedure in Ref. [10]. In this context see also the original approach for plane stress of Pian and Sumihara [29] with $\bar{\xi} = \bar{\eta} = 0$ and the text book Zienkiewicz and Taylor, part 1, [30]. Finally we mention Ref. [20], where the shear approximation is performed in a more complicated way.

The constants $\bar{\xi}$ and $\bar{\eta}$ are introduced to obtain decoupled matrices in the below defined matrix $\mathbf{H}$ and denote the coordinates of the center of gravity of the element.

$$
\bar{\xi} = \frac{1}{A_e}\int\limits_{(\Omega_e)} \xi\, dA = \frac{1}{3}\frac{j_1}{j_0} \qquad\qquad \bar{\eta} = \frac{1}{A_e}\int\limits_{(\Omega_e)} \eta\, dA = \frac{1}{3}\frac{j_2}{j_0} \tag{23}
$$

The element area is given by $A_e = 4j_0$. The transformation coefficients in (22) are the components of the Jacobian matrix $\mathbf{J}$ according to (19), evaluated at the element center $J_{\alpha\beta}^0 = J_{\alpha\beta}(\xi = 0, \eta = 0)$. The coefficients have to be constant in order to fulfill the patch test, see e.g. [30].

3.5 Analytical Integration of the Element Matrices

Inserting the finite element equations (9)- (23) and the corresponding equations for the virtual stresses and virtual strains into the stationary condition (7) yields

$$
\delta\Pi_{HR}^h = \sum_{e=1}^{numel} \begin{bmatrix} \delta\boldsymbol{\beta} \\ \delta\mathbf{v} \end{bmatrix}_e^T \left\{ \begin{bmatrix} -\mathbf{H} & \mathbf{G} \\ \mathbf{G}^T & \mathbf{0} \end{bmatrix} \begin{bmatrix} \boldsymbol{\beta} \\ \mathbf{v} \end{bmatrix} - \begin{bmatrix} \mathbf{0} \\ \mathbf{p} \end{bmatrix} \right\}_e = 0\,, \tag{24}
$$

where *numel* denotes the total number of shell elements to discretize the problem. Here, $\mathbf{v} = [\mathbf{v}_1, \mathbf{v}_2, \mathbf{v}_3, \mathbf{v}_4]^T$ is the element displacement vector and and $\delta\mathbf{v}\,, \delta\boldsymbol{\beta}$ the corresponding virtual element vectors, respectively. The element load vector $\mathbf{p} = [\mathbf{p}_1, \mathbf{p}_2, \mathbf{p}_3, \mathbf{p}_4]^T$ which follows from the external virtual work is identical with a pure displacement formulation.

Furthermore the matrices $\mathbf{H}$ and $\mathbf{G}$ are introduced with $\mathbf{B} = [\mathbf{B}_1, \mathbf{B}_2, \mathbf{B}_3, \mathbf{B}_4]$,

$$\mathbf{H} = \int_{(\Omega_e)} \mathbf{S}^T \mathbf{C}^{-1} \mathbf{S} \, dA \,, \qquad \mathbf{G} = \int_{(\Omega_e)} \mathbf{S}^T \mathbf{B} \, dA \,. \tag{25}$$

Since the integrand in $(25)_1$ involves only polynomials of the coordinates ξ and η the integration can be carried out analytically. In this context we also refer to the expressions for a plate in [28]. Due to the introduced constants $\bar{\xi}$ and $\bar{\eta}$ one obtains a matrix $\mathbf{H}$ only with diagonal entries

$$\mathbf{H} = \begin{bmatrix} A_e \, \mathbf{C}^{-1} & \mathbf{0} \\ \mathbf{0} & \mathbf{h} \end{bmatrix} \qquad \text{with} \qquad \mathbf{h} = \begin{bmatrix} \mathbf{h}^m & \mathbf{0} & \mathbf{0} \\ \mathbf{0} & \mathbf{h}^b & \mathbf{0} \\ \mathbf{0} & \mathbf{0} & \mathbf{h}^s \end{bmatrix}_{(6\times 6)} \,. \tag{26}$$

The components of the symmetric sub-matrices $\mathbf{h}^m$, $\mathbf{h}^b = 12\,\mathbf{h}^m/h^2$ and $\mathbf{h}^s$ are given with

$$\begin{aligned}
h^m_{11} &= \frac{A_e f_{11}}{3Eh} \, (J^{02}_{11} + J^{02}_{12})^2 \\
h^m_{22} &= \frac{A_e f_{22}}{3Eh} \, (J^{02}_{21} + J^{02}_{22})^2 \\
h^m_{12} &= h^m_{21} = \frac{A_e f_{12}}{3Eh} \, \left[(J^0_{11} \, J^0_{21} + J^0_{22} J^0_{12})^2 - \nu \, (J^0_{11} \, J^0_{22} - J^0_{12} J^0_{21})^2 \right] \\
h^s_{11} &= \frac{A_e f_{11}}{3\kappa G h} \, (J^{02}_{11} + J^{02}_{12}) \\
h^s_{22} &= \frac{A_e f_{22}}{3\kappa G h} \, (J^{02}_{21} + J^{02}_{22}) \\
h^s_{12} &= h^s_{21} = \frac{A_e f_{12}}{3\kappa G h} \, (J^0_{11} \, J^0_{21} + J^0_{22} J^0_{12}) \,.
\end{aligned} \tag{27}$$

$$\begin{aligned}
f_{11} &= 1 - \frac{1}{3} \left(\frac{j_2}{j_0} \right)^2 \\
f_{22} &= 1 - \frac{1}{3} \left(\frac{j_1}{j_0} \right)^2 \\
f_{12} &= -\frac{1}{3} \frac{j_1}{j_0} \frac{j_2}{j_0}
\end{aligned}$$

The matrix $\mathbf{G}$ according to $(25)_2$ can only be integrated analytically in Ω^h_0. For this reason we replace in (17) the base vectors $\mathbf{X}_{,\alpha}$ by $\mathbf{t}_\alpha$, introduce $\mathbf{b}^0_{\alpha I} = \mathbf{W}_I \, \mathbf{t}_\alpha$ and replace $\mathbf{D}_{,\alpha}$ by $\mathbf{D}^0_{,\alpha}$ evaluated at the element center

$$\begin{bmatrix} \mathbf{D}^{0T}_{,1} \\ \mathbf{D}^{0T}_{,2} \end{bmatrix} = \frac{1}{4} \, \mathbf{J}^{0-1} \begin{bmatrix} -\mathbf{D}^T_1 + \mathbf{D}^T_2 + \mathbf{D}^T_3 - \mathbf{D}^T_4 \\ -\mathbf{D}^T_1 - \mathbf{D}^T_2 + \mathbf{D}^T_3 + \mathbf{D}^T_4 \end{bmatrix} \,, \quad \mathbf{J}^0 = \mathbf{J}(\xi = \eta = 0) \,. \tag{28}$$

These assumptions have consequences on the element behaviour, which are discussed in the next section. With the simplifications $\mathbf{G}_0$ is obtained by analytical integration, where the

subscript 0 refers to the flat projection Ω_0^h

$$\mathbf{G}_0 = [\mathbf{G}_{01}, \mathbf{G}_{02}, \mathbf{G}_{03}, \mathbf{G}_{04}] \qquad \mathbf{G}_{0I} = \begin{bmatrix} A_e\, \mathbf{B}_{0I}^0 \\ \mathbf{g}_{0I} \end{bmatrix} \tag{29}$$

where

$$\mathbf{B}_{0I}^0 = \begin{bmatrix} N_I^0{}_{,1}\ \mathbf{t}_1^T & \mathbf{0} \\ N_I^0{}_{,2}\ \mathbf{t}_2^T & \mathbf{0} \\ N_I^0{}_{,1}\ \mathbf{t}_2^T + N_I^0{}_{,2}\ \mathbf{t}_1^T & \mathbf{0} \\ N_I^0{}_{,1}\ \mathbf{D}_{,1}^{0T} & N_I^0{}_{,1}\ \mathbf{b}_{1I}^{0T} \\ N_I^0{}_{,2}\ \mathbf{D}_{,2}^{0T} & N_I^0{}_{,2}\ \mathbf{b}_{2I}^{0T} \\ N_I^0{}_{,1}\ \mathbf{D}_{,2}^{0T} + N_I^0{}_{,2}\ \mathbf{D}_{,1}^{0T} & N_I^0{}_{,1}\ \mathbf{b}_{2I}^{0T} + N_I^0{}_{,2}\ \mathbf{b}_{1I}^{0T} \\ \mathbf{J}^{0-1} \left\{ \begin{array}{c} a_{1I}\, \mathbf{D}_M^T \\ a_{2I}\, \mathbf{D}_L^T \end{array} \right\} & \frac{1}{4}\, \mathbf{J}^{0-1} \left\{ \begin{array}{c} \mathbf{b}_M^T \\ \mathbf{b}_L^T \end{array} \right\} \end{bmatrix} \tag{30}$$

$$\begin{bmatrix} N_I^0{}_{,1} \\ N_I^0{}_{,2} \end{bmatrix} = \mathbf{J}^{0-1} \begin{bmatrix} a_{1I} \\ a_{2I} \end{bmatrix}$$

and

$$\mathbf{g}_{0I} = \frac{A_e}{3}\gamma_I \begin{bmatrix} J_{11}^0\, \mathbf{t}_1^T + J_{12}^0\, \mathbf{t}_2^T & \mathbf{0} \\ J_{21}^0\, \mathbf{t}_1^T + J_{22}^0\, \mathbf{t}_2^T & \mathbf{0} \\ J_{11}^0\, \mathbf{D}_{,1}^{0T} + J_{12}^0\, \mathbf{D}_{,2}^{0T} & J_{11}^0\, \mathbf{b}_{1I}^{0T} + J_{12}^0\, \mathbf{b}_{2I}^{0T} \\ J_{21}^0\, \mathbf{D}_{,1}^{0T} + J_{22}^0\, \mathbf{D}_{,2}^{0T} & J_{21}^0\, \mathbf{b}_{1I}^{0T} + J_{22}^0\, \mathbf{b}_{2I}^{0T} \\ \gamma_I^{11}\, \mathbf{D}_M^T + \gamma_I^{12}\, \mathbf{D}_L^T & \gamma_I^{11}\, \xi_I\, \mathbf{b}_M^T + \gamma_I^{12}\, \eta_I\, \mathbf{b}_L^T \\ \gamma_I^{21}\, \mathbf{D}_M^T + \gamma_I^{22}\, \mathbf{D}_L^T & \gamma_I^{21}\, \xi_I\, \mathbf{b}_M^T + \gamma_I^{22}\, \eta_I\, \mathbf{b}_L^T \end{bmatrix} \tag{31}$$

$$\begin{aligned} \gamma_I &= h_I - \frac{j_2}{j_0} a_{1I} - \frac{j_1}{j_0} a_{2I} \\ \gamma_I^{11} &= (h_I - \frac{j_2}{j_0} a_{1I})/\gamma_I & \gamma_I^{12} &= -\frac{j_1}{j_0} a_{2I}/\gamma_I \\ \gamma_I^{21} &= -\frac{j_2}{j_0} a_{1I}/\gamma_I & \gamma_I^{22} &= (h_I - \frac{j_1}{j_0} a_{2I})/\gamma_I\,. \end{aligned}$$

3.6 Transformation of the Element Matrices

Since the interpolation of the stress resultants are discontinuous at the element boundaries and with $\delta\mathbf{v} \neq \mathbf{0}$, $\delta\boldsymbol{\beta} \neq \mathbf{0}$, the parameters $\boldsymbol{\beta}$ can be eliminated on the element level considering (24)

$$\boldsymbol{\beta} = \mathbf{H}^{-1}\mathbf{G}\,\mathbf{v}\,. \tag{32}$$

Hence the stationary condition (24) reads

$$\delta\Pi^h_{HR} = \sum_{e=1}^{numel} \delta\mathbf{v}^T\mathbf{S} = \sum_{e=1}^{numel} \delta\mathbf{v}_0^T\mathbf{S}_0 = 0\,, \qquad \begin{aligned} \mathbf{S} &= \mathbf{G}^T\,\mathbf{H}^{-1}\,\mathbf{G}\,\mathbf{v} - \mathbf{p} \\ \mathbf{S}_0 &= \mathbf{G}_0^T\,\mathbf{H}^{-1}\,\mathbf{G}_0\,\mathbf{v}_0 - \mathbf{p}_0\,. \end{aligned} \tag{33}$$

The assembly can be performed as within a pure displacement formulation. However, at first the nodal force vector $\mathbf{S}_0 = [\mathbf{S}_{01}, \mathbf{S}_{02}, \mathbf{S}_{03}, \mathbf{S}_{04}]^T$ has to be transformed considering the distance vector $\mathbf{r}_I$ between Ω_0^h and Ω^h at the nodes, see Fig. 1 and Ref. [27]

$$\mathbf{r}_I = z_I\,\mathbf{t}_3\,, \qquad z_I = (\mathbf{X}_I - \mathbf{X}_0)\cdot\mathbf{t}_3 = \pm\bar{h}\,, \qquad \mathbf{X}_0 = \frac{1}{4}\sum_{I=1}^{4}\mathbf{X}_I\,. \tag{34}$$

The equilibrium equations read with $\bar{\mathbf{W}}_I = \operatorname{skew}\mathbf{r}_I$ defined by $\mathbf{r}_I \times \mathbf{f}_I = \bar{\mathbf{W}}_I\,\mathbf{f}_I$

$$\begin{aligned} \begin{bmatrix} \mathbf{f}_{0I} \\ \mathbf{m}_{0I} \end{bmatrix} &= \begin{bmatrix} \mathbf{1}_3 & \mathbf{0} \\ \bar{\mathbf{W}}_I & \mathbf{1}_3 \end{bmatrix} \begin{bmatrix} \mathbf{f}_I \\ \mathbf{m}_I \end{bmatrix} \\ \mathbf{S}_{0I} &= \mathbf{T}_{SI}\,\mathbf{S}_I\,. \end{aligned} \tag{35}$$

The corresponding transformations for the displacements and virtual displacements can be derived from the virtual work (33)

$$\begin{aligned} \begin{bmatrix} \mathbf{u}_{0I} \\ \boldsymbol{\varphi}_{0I} \end{bmatrix} &= \begin{bmatrix} \mathbf{1}_3 & \bar{\mathbf{W}}_I \\ \mathbf{0} & \mathbf{1}_3 \end{bmatrix} \begin{bmatrix} \mathbf{u}_I^G \\ \boldsymbol{\varphi}_I^G \end{bmatrix} \\ \mathbf{v}_{0I} &= \mathbf{T}_{1I}\,\mathbf{v}_I^G\,. \end{aligned} \tag{36}$$

It should be noted that without transformation (36) the element is unacceptable stiff for warped configurations, see also [27].

At the nodes which are not positioned on intersections no drilling stiffness is available and a second transformation of the stiffness and the load vector is necessary:

$$\begin{aligned} \begin{bmatrix} \mathbf{u}_I^G \\ \boldsymbol{\varphi}_I^G \end{bmatrix} &= \begin{bmatrix} \mathbf{1}_3 & \mathbf{0} \\ \mathbf{0} & \mathbf{T}_{3I} \end{bmatrix} \begin{bmatrix} \mathbf{u}_I^G \\ \boldsymbol{\varphi}_I^L \end{bmatrix} \\ \mathbf{v}_I^G &= \mathbf{T}_{2I}\,\mathbf{v}_I \\ \mathbf{T}_{3I} &= \begin{cases} \mathbf{1}_3 & \text{for nodes on shell intersections} \\ [\mathbf{a}_{1I}, \mathbf{a}_{2I}]_{(3\times 2)} & \text{for all other nodes} \end{cases} \end{aligned} \tag{37}$$

At all nodes which are not positioned on intersections the drilling degree of freedom is fixed. Thus the element possesses six degrees of freedom at all nodes on intersections and five at all other nodes. In this context we also refer to [31, 32].

Combining (36) and (37) with (33) yields the total transformation $\mathbf{T}_I = \mathbf{T}_{1I}\,\mathbf{T}_{2I}$ and

$$\mathbf{G}_I = \mathbf{G}_{0I}\,\mathbf{T}_I = \begin{bmatrix} A_e\mathbf{B}^0_I \\ \mathbf{g}_I \end{bmatrix}$$

$$\mathbf{B}^0_I = \begin{bmatrix} N^0_{I,1}\,\mathbf{t}^T_1 & N^0_{I,1}\,\bar{\mathbf{b}}^T_{1I} \\ N^0_{I,2}\,\mathbf{t}^T_2 & N^0_{I,2}\,\bar{\mathbf{b}}^T_{2I} \\ N^0_{I,1}\,\mathbf{t}^T_2 + N^0_{I,2}\,\mathbf{t}^T_1 & N^0_{I,1}\,\bar{\mathbf{b}}^T_{2I} + N^0_{I,2}\,\bar{\mathbf{b}}^T_{1I} \\ N^0_{I,1}\,\mathbf{D}^{0T}_{,1} & N^0_{I,1}\,\tilde{\mathbf{b}}^T_{1I} \\ N^0_{I,2}\,\mathbf{D}^{0T}_{,2} & N^0_{I,2}\,\tilde{\mathbf{b}}^T_{2I} \\ N^0_{I,1}\,\mathbf{D}^{0T}_{,2} + N^0_{I,2}\,\mathbf{D}^{0T}_{,1} & N^0_{I,1}\,\tilde{\mathbf{b}}^T_{2I} + N^0_{I,2}\,\tilde{\mathbf{b}}^T_{1I} \\ \mathbf{J}^{0-1}\begin{Bmatrix} a_{1I}\,\mathbf{D}^T_M \\ a_{2I}\,\mathbf{D}^T_L \end{Bmatrix} & \mathbf{J}^{0-1}\begin{Bmatrix} \tilde{\mathbf{b}}^T_M \\ \tilde{\mathbf{b}}^T_L \end{Bmatrix} \end{bmatrix}$$

$$\mathbf{g}_I = \frac{A_e}{3}\gamma_I \begin{bmatrix} J^0_{11}\,\mathbf{t}^T_1 + J^0_{12}\,\mathbf{t}^T_2 & J^0_{11}\,\bar{\mathbf{b}}^T_{1I} + J^0_{12}\,\bar{\mathbf{b}}^T_{2I} \\ J^0_{21}\,\mathbf{t}^T_1 + J^0_{22}\,\mathbf{t}^T_2 & J^0_{21}\,\bar{\mathbf{b}}^T_{1I} + J^0_{22}\,\bar{\mathbf{b}}^T_{2I} \\ J^0_{11}\,\mathbf{D}^{0T}_{,1} + J^0_{12}\,\mathbf{D}^{0T}_{,2} & J^0_{11}\,\tilde{\mathbf{b}}^T_{1I} + J^0_{12}\,\tilde{\mathbf{b}}^T_{2I} \\ J^0_{21}\,\mathbf{D}^{0T}_{,1} + J^0_{22}\,\mathbf{D}^{0T}_{,2} & J^0_{21}\,\tilde{\mathbf{b}}^T_{1I} + J^0_{22}\,\tilde{\mathbf{b}}^T_{2I} \\ \gamma^{11}_I\,\mathbf{D}^T_M + \gamma^{12}_I\,\mathbf{D}^T_L & \gamma^{11}_I\,\hat{\mathbf{b}}^T_M + \gamma^{12}_I\,\hat{\mathbf{b}}^T_L \\ \gamma^{21}_I\,\tilde{\mathbf{D}}^T_M + \gamma^{22}_I\,\tilde{\mathbf{D}}^T_L & \gamma^{21}_I\,\hat{\mathbf{b}}^T_M + \gamma^{22}_I\,\hat{\mathbf{b}}^T_L \end{bmatrix} \tag{38}$$

$$\begin{aligned}
\bar{\mathbf{b}}_{\alpha I} &= \mathbf{T}^T_{4I}\,\mathbf{t}_\alpha \\
\tilde{\mathbf{b}}_{\alpha I} &= \mathbf{T}^T_{4I}\,\mathbf{D}^0{}_{,\alpha} + \mathbf{T}^T_{3I}\,\mathbf{b}^0_{\alpha I} \\
\tilde{\mathbf{b}}_M &= \tfrac{1}{4}\left(\xi_I\,\mathbf{T}^T_{4I}\,\mathbf{D}_M + \mathbf{T}^T_{3I}\,\mathbf{b}_M\right) \\
\tilde{\mathbf{b}}_L &= \tfrac{1}{4}\left(\eta_I\,\mathbf{T}^T_{4I}\,\mathbf{D}_L + \mathbf{T}^T_{3I}\,\mathbf{b}_L\right) \\
\hat{\mathbf{b}}_M &= \mathbf{T}^T_{4I}\,\mathbf{D}_M + \xi_I\,\mathbf{T}^T_{3I}\,\mathbf{b}_M \\
\hat{\mathbf{b}}_L &= \mathbf{T}^T_{4I}\,\mathbf{D}_L + \eta_I\,\mathbf{T}^T_{3I}\,\mathbf{b}_L\,.
\end{aligned}$$

with $\mathbf{T}_{4I} = \bar{\mathbf{W}}_I\,\mathbf{T}_{3I}$. For a constant load $\bar{\mathbf{p}} = \bar{p}_i\mathbf{e}_i$ in Ω we obtain

$$\mathbf{p}_I = \mathbf{T}^T_I\,\mathbf{p}_{0I} = A_e\left(a_{0I} + \frac{1}{3}\frac{j_1}{j_0}a_{1I} + \frac{1}{3}\frac{j_2}{j_0}a_{2I}\right)\begin{bmatrix} \bar{\mathbf{p}} \\ \mathbf{T}^T_{4I}\,\bar{\mathbf{p}} \end{bmatrix}. \tag{39}$$

Thus considering (26), (33) and (38) the element stiffness matrix reads

$$\begin{aligned}
\mathbf{k}^e &= \mathbf{G}^T\mathbf{H}^{-1}\mathbf{G} = \mathbf{k}_0 + \mathbf{k}_{stab} \\
\mathbf{k}_{IK} &= \mathbf{G}^T_I\,\mathbf{H}^{-1}\,\mathbf{G}_K = A_e\mathbf{B}^{0T}_I\mathbf{C}\mathbf{B}^0_K + \mathbf{g}^T_I\mathbf{h}^{-1}\mathbf{g}_K\,.
\end{aligned} \tag{40}$$

Here, $\mathbf{k}_0$ denotes the stiffness of a one–point integrated Reissner–Mindlin shell element with assumed shear strains and $\mathbf{k}_{stab}$ the stabilization matrix. The matrix $\mathbf{h}$ according to (26) consists of three submatrices of order two and thus can easily be inverted. The element stiffness matrix possesses with six zero eigenvalues the correct rank.

4 Examples

The derived element formulation has been implemented in an extended version of the general purpose finite element program FEAP, see Zienkiewicz and Taylor [30].

4.1 Membrane and bending patch test

Here we investigate a rectangular plate under membrane forces and bending moments according to [33]. Both, membrane and bending patch test are fulfilled by the present element.

4.2 Corner supported square plate

A corner supported plate with edge length $2a$ subjected to uniform load is discussed. Considering symmetry the mesh consists of 8×8 elements for a quarter of the plate, see Fig. 2. The geometrical and material data are also given. An approximate ansatz according to [34] reads

$$w(x,y) = c_1 + c_2 x^2 + c_3 y^2 + c_4 x^4 + c_5 x^2 y^2 + c_6 y^4 \,, \tag{41}$$

where the origin of the co-ordinate system lies in the center of the plate. The boundary condition of vanishing bending moments at the edges can only be fulfilled in an integral sense. The other boundary conditions and the partial differential equation can be fulfilled exactly. The constants are determined and thus for $y = 0$ the approximate Kirchhoff solution reads

$$w(x, y=0) = \frac{qa^4}{2Eh^3}[11 - 6\nu - \nu^2 + (-5 + 4\nu + \nu^2)(\frac{x}{a})^2 + (1 + \frac{\nu}{2} - \frac{\nu^2}{2})(\frac{x}{a})^4] \,. \tag{42}$$

$$\begin{aligned} a &= 12 \\ h &= 0.375 \\ q &= 0.03125 \\ E &= 430000 \\ \nu &= 0.38 \end{aligned}$$

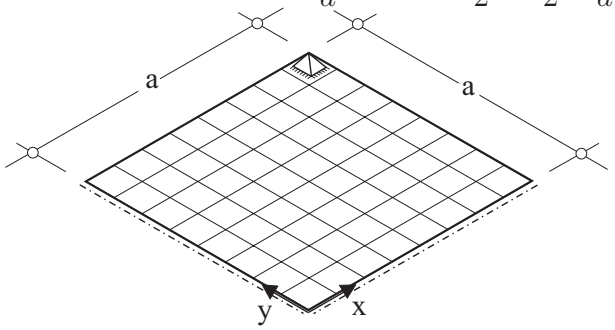

Figure 2: Corner supported plate

The deflections $w(x, y = 0)$ obtained with different elements are plotted in Fig. 3. The Belytschko/Tsay element [13] leads to hourglass modes for parameters $r_w < 0.02$, optimal results for $0.02 \leq r_w \leq 0.05$ and locking for $r_w > 0.05$, see also [13] and Fig. 3. The parameter $r_\beta = 0.02$ has been chosen constant in all cases.

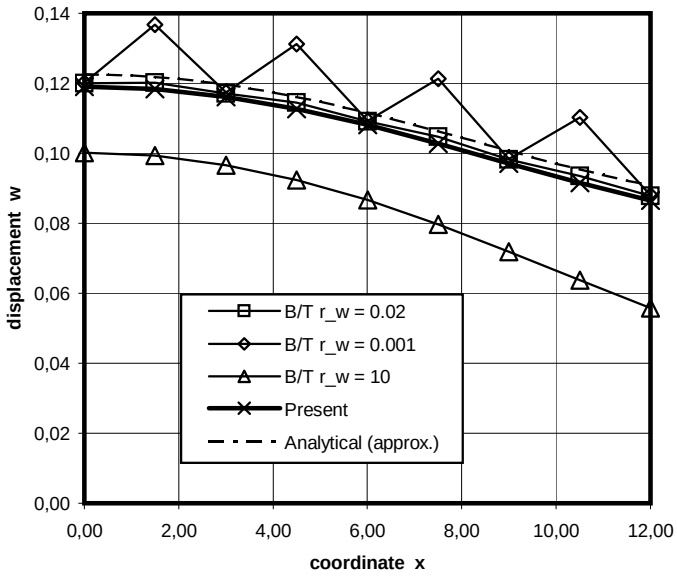

Figure 3: Deflection $w(x, y = 0)$ for the corner supported plate, comparison of different elements

4.3 Hemispherical shell with a 18° hole

The hemispherical shell with a 18° hole under opposite loads is a standard example in linear and nonlinear shell analysis. The material properties are $E = 6.825 \cdot 10^7$ and $\nu = 0.3$, the radius is $R = 10$ and the thickness is $h = 0.04$. Considering symmetry conditions a quarter of the shell is modelled with a regular mesh, see Fig. 4. Table 1 presents results for the displacement of the loaded node for different elements. The values are normalized with respect to our converged solution $w = 0.0935$ for $F = 1$. Analytical solutions based on asymptotic expansions are reported in [10] with $w = 0.093$. In Ref. [33] a value of $w = 0.094$ has been used for normalization. It can be seen that the results obtained with the present element as well as the results using the elements [27], [23] converge against the same solution. For this example the convergence behaviour of the investigated elements is practically the same.

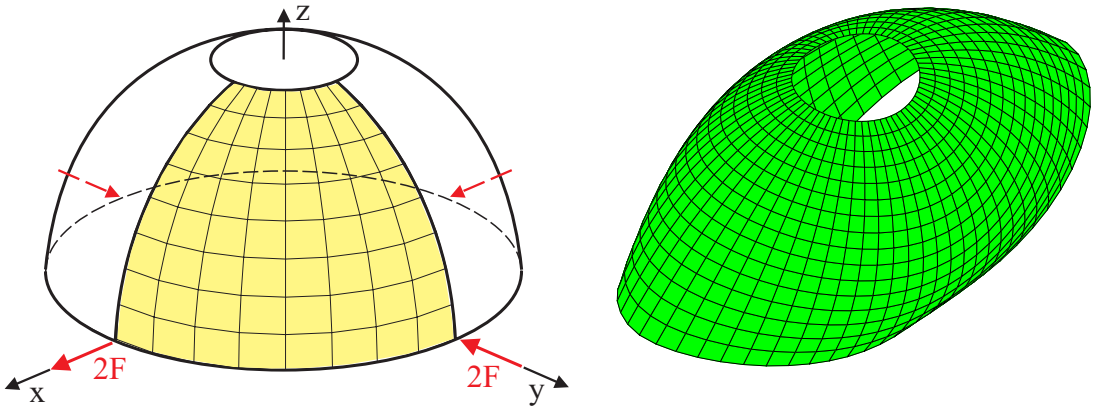

Figure 4: Hemispherical shell: Un-deformed and deformed mesh (amplified by a factor 50)

Table 1: Normalized displacements for different elements

Nodes per side	Simo[10]	Taylor [27]	Sauer [23]	Present
3	91.4	*66.1	106.7	106.2
5	99.9	92.5	103.8	103.8
9	99.3	100.7	100.3	100.4
17	99.4	100.0	99.8	99.8
33	-	*100.0	100.0	100.0

* Own results using the element of Taylor [27].

4.4 Full hemispherical shell

The convergence behaviour using distorted and warped elements is investigated with the hemispherical shell of the last section without the hole. The results for the deflections in load direction are normalized with respect to our converged numerical solution $w = 0.09227$,

see Table 2. In Ref. [10] a reference value of 0.0924 is given. The elements [23], [27] and the present element converge against the same solution. The deformed mesh along with the radial displacements is plotted in Fig. 5.

Table 2: Normalized displacements for different elements

Nodes per side	Simo[10] mixed	Simo[10] disp	Taylor[27]*	Sauer[23]	Present
5	65.2	46.9	77.0	50.5	57.4
9	96.9	93.4	100.8	95.5	97.2
17	99.4	98.9	100.8	100.0	100.3
33	-	-	100.2	100.0	100.1
65	-	-	100.0	100.0	100.0

* Own results using the element of Taylor [27].

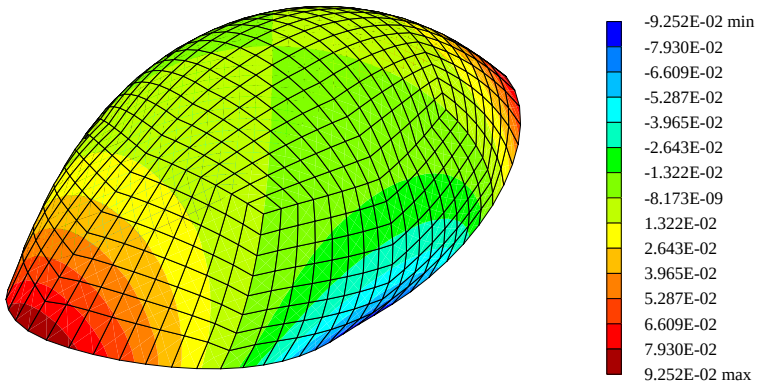

Figure 5: Radial displacements and deformed mesh (amplified by a factor 50)

4.5 Twisted beam

This problem, a clamped beam twisted 90° subjected to two different concentrated loads at the tip, was originally introduced by MacNeal and Harder [33]. A more demanding thin shell version was proposed by Jetteur [35] and is investigated in this paper. The example is chosen to test the assess of warping on the performance of shell elements. Two load cases are discussed. Load case 1 is a unit shear load in width direction whereas load case 2 is a unit shear load in thickness direction, see Fig. 6. The computed tip displacements in load direction are normalized with respect to our converged solutions 1.387 (load case 1) and 0.343 (load case 2) and are presented in Tab. 3. The displacements u_z and u_y are plotted for the respective load case on the deformed configurations in Fig. 7.

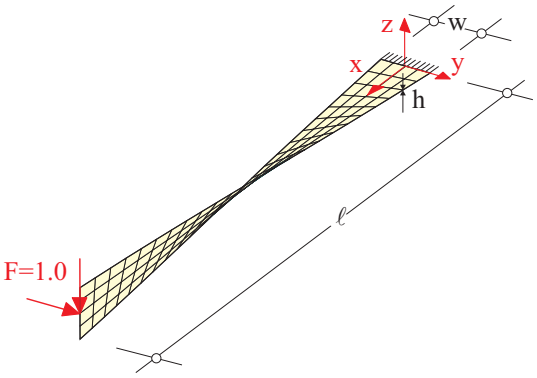

$$
\begin{aligned}
l &= 12 \\
w &= 1.1 \\
h &= 0.05 \\
E &= 29 \cdot 10^6 \\
\nu &= 0.22 \\
F &= 1.0
\end{aligned}
$$

Figure 6: Twisted beam: geometrical and material data

Table 3: Load case 1 normalized displacement u_z for different elements

Mesh	El.	Simo[10]	Taylor[27]	Sauer[23]	Present
1*6	6	99.4	100.1	99.5	102.0
2*12	24	100.0	100.2	99.7	100.6
4*24	96	100.1	100.1	99.9	99.3
8*48	384	100.2	100.0	100.0	100.0

Table 4: Load case 2 normalized displacement u_y for different elements

Mesh	El.	Simo[10]	Taylor[27]	Sauer[23]	Present
1*6	6	95.1	102.1	94.0	104.3
2*12	24	98.6	101.0	98.4	100.5
4*24	96	99.7	100.2	99.6	99.3
8*48	384	100.0	100.0	99.9	100.0

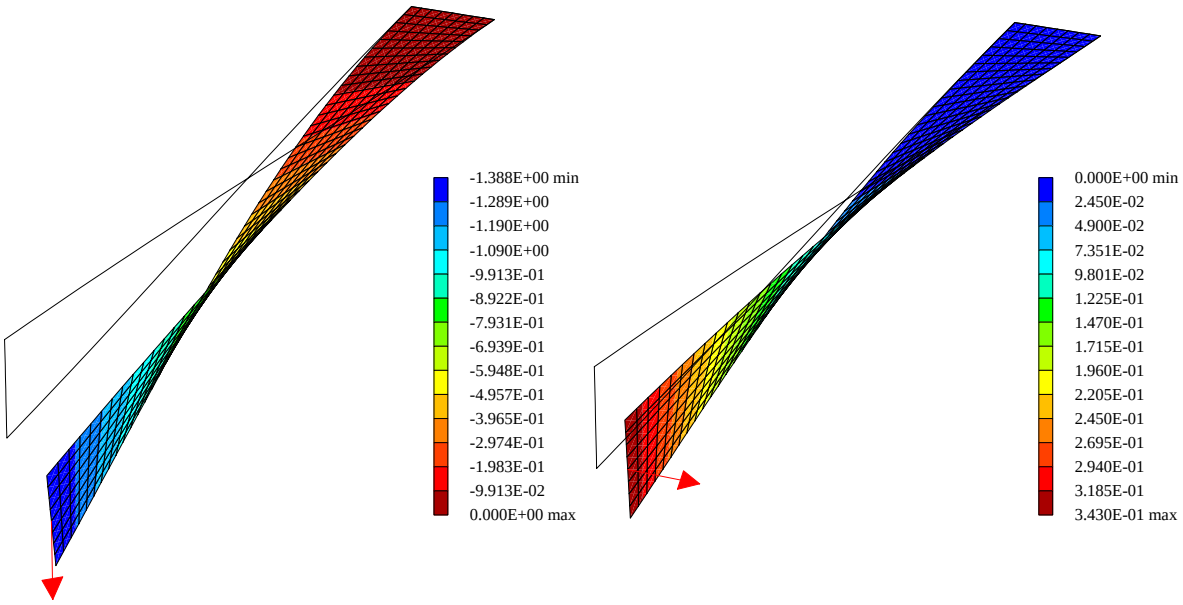

Figure 7: Deformed configurations for load case 1 and 2 and respective displacements u_z and u_y

4.6 Hypar shell

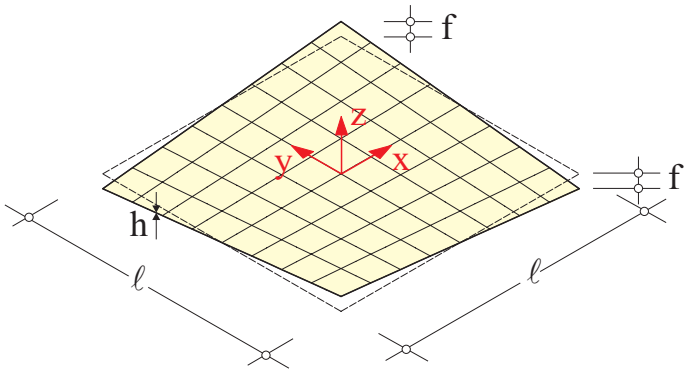

$$
\begin{array}{lcll}
l & = & 20 & m \\
f & = & l/32 & m \\
h & = & 0.2 & m \\
E & = & 10^8 & kN/m^2 \\
\nu & = & 0 & \\
\bar{p}_z & = & -5 & kN/m^2
\end{array}
$$

Figure 8: Hypar shell: geometrical and material data

The geometry of the considered hyperbolic paraboloid shell is described by the function $z = 1/8\,xy$. The shell is loaded by a constant load $\bar{p}_z$ per shell middle surface in vertical direction. Along the boundary the deflections are restrained in global z–direction. Furthermore the boundary conditions $u_x(-l/2, 0) = u_x(l/2, 0) = 0$ and $u_y(0, -l/2) = u_y(0, l/2) = 0$ are considered. An analytical Kirchhoff solution with slightly different boundary conditions using Fourier series has been derived by Duddeck [36]. The shell with coordinates $z(l/2, l/2) = \pm f = l/32$ is rather flat. Therefore the support perpendicular to the shell which has been considered in [36] does not lead to significant different results. The geometrical and material data as well as a typical finite element mesh are depicted in Fig. 8. The distribution of the global displacement $w = u_z$ is symmetric with respect to $x = 0$ and $y = 0$. In Fig. 9 the deflection w $(0 < x < l/2, y = 0)$ is depicted. The calculated results are in good agreement with the solution of Duddeck. Furthermore the distribution of the bending moment m_{xy} $(0 < x < l/2, y = l/2)$ is presented in this Figure. Differences occur along the edges due to the fact that the analytical solution is based on a Kirchhoff theory whereas the numerical solution is calculated using the Reissner–Mindlin theory. In Fig. 10 the distribution of the bending moment m_x $(0 < x < l/2, y = 0)$ and m_x $(x = 0, 0 < y < l/2)$ are shown. The good agreement with the analytical solution is noted.

Table 5: Center displacement $w(0, 0)$ in cm for different elements

Nodes per Side	$w(0,0)$			
	Taylor [27]*	Sauer [23]	Present	Duddeck [36]
2	4.05	2.84	4.03	
4	4.42	4.39	4.41	
8	4.51	4.51	4.52	
17	4.55	4.56	4.56	
33	4.56	4.58	4.58	
65	4.57	4.60	4.60	4.6

* Own results with the element of Taylor [27].

Finally a convergence study is presented in Tables 5 and 6 for the center deflection $w(0,0)$ and the bending moment $m_x(0,0)$, respectively. It shows that the present element exhibits a superior convergence behaviour for the bending moment.

Table 6: Center moment $m_x(0,0)$ in kNm/m for different elements

Nodes per Side	$m_x(0,0)$			
	Taylor [27]*	Sauer [23]	Present	Duddeck [36]
2	36.0	25.2	53.6	
4	57.7	60.2	64.0	
8	62.6	63.3	64.3	
17	64.3	64.6	64.9	
33	64.8	65.0	65.1	
65	64.9	65.3	65.3	63

* Own results with the element of Taylor [27].

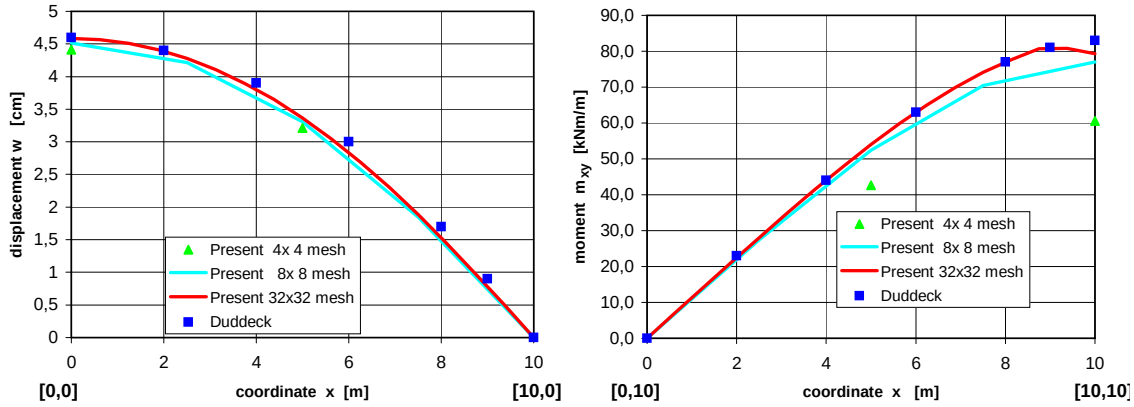

Figure 9: Displacement $w(x, y \mid 0 < x < l/2, y = 0)$ and bending moment $m_{xy}(x, y \mid 0 < x < l/2, y = l/2)$

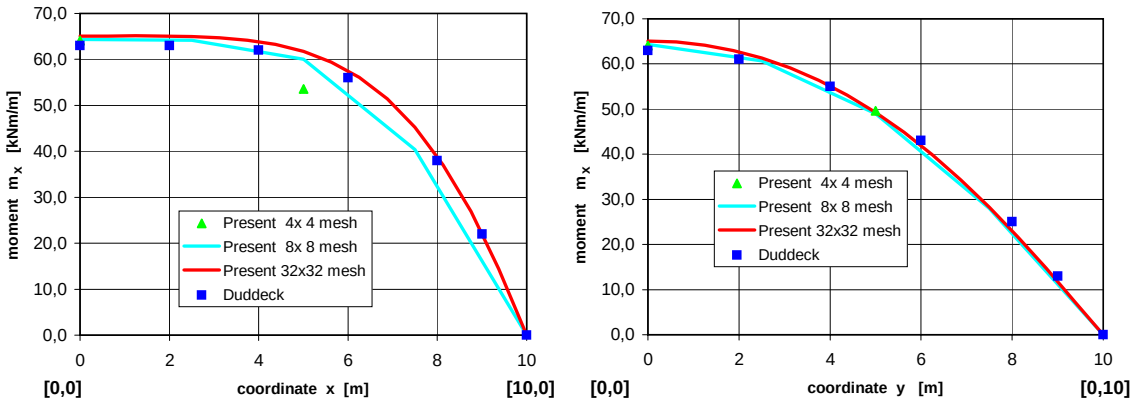

Figure 10: Bending moment $m_x(x, y \mid 0 < x < l/2, y = 0)$ and $m_x(x, y \mid x = 0, 0 < y < l/2)$

4.7 Steel frame structure

In the last example we discuss a symmetrical frame structure with welded cross–sections, see Figs. 11, 12. Thus, different intersections of plates occur, which can be treated with the present model. The frame is loaded by a constant vertical load $\bar{p} = 16\ kN/m$. The problem with all geometrical data as well as the load distribution is presented in Fig. 11, the underlying data for the cross–sections of a beam model are depicted in Fig. 12. Elastic material behaviour is assumed using the parameters $E = 21000\ kN/cm^2$ and $\nu = 0.3$.

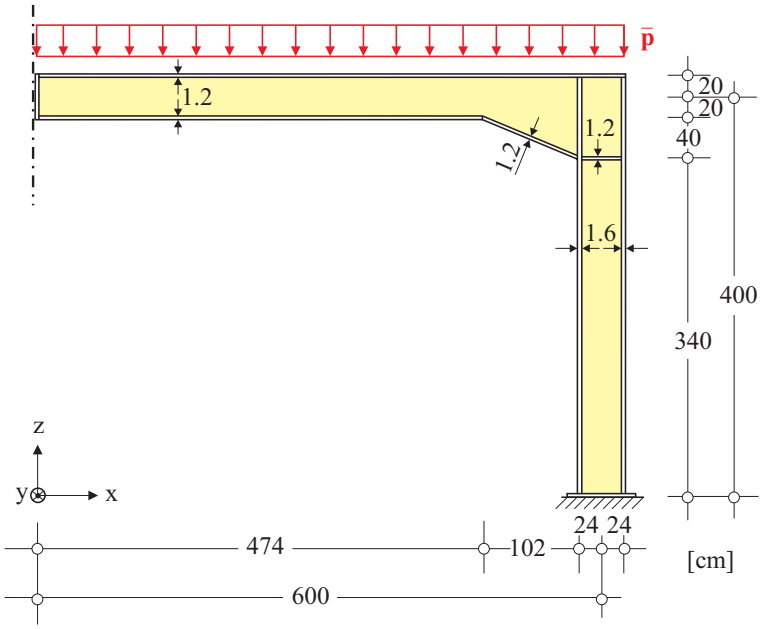

Figure 11: Frame structure: system and loading

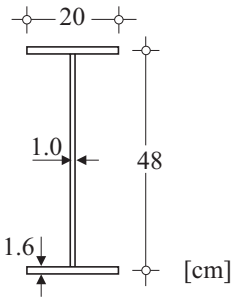

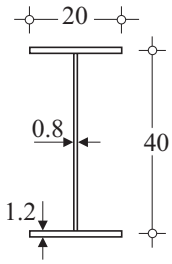

frame column			horizontal member		
A	=	$112.0\ cm^2$	A	=	$80.0\ cm^2$
I_y	=	$46094\ cm^4$	I_y	=	$23472\ cm^4$
I_z	=	$2137\ cm^4$	I_z	=	$1602\ cm^4$
I_T	=	$70.6\ cm^4$	I_T	=	$29.9\ cm^4$

Figure 12: Definition of cross sections

The finite element calculations are performed with the developed shell element using a mesh with 530 nodes and 368 elements, see Fig. 13, and for comparison with 15 two–dimensional beam elements, see Fig. 17. It can be seen from Tables 7 and 8 that the results of all used three shell elements are very similar for the vertical displacement $u_z(0, 0, 400)$ in the symmetry plane as well as for the stresses σ_{11} in axial direction at the coordinates $(0, 0, 420)$ and $(0, 0, 380)$. This could also be verified using the beam model with only little deviations. In detail Fig. 13 show the un–deformed and deformed mesh, whereas the axial

stresses σ_{11} at the plate mid–surfaces are depicted in Figs. 15 and 16. Finally Fig. 17 presents the associated results for the beam model. Here, normal forces of $N = -72.6\ kN$ and $N = -96.0\ kN$ occur in the horizontal member and the column of the frame. It should be noted that only the shell model is able to analyze the stress state in the corner of the frame (see Fig. 16).

Table 7: Vertical displacement $u_z(0, 0, 400)$ in cm

Displacement u_z	Taylor[27]	Sauer[23]	Present
Shell model	-1.818	-1.817	-1.817
Beam model			-1.761

Table 8: Axial stresses σ_{11} in symmetry plane in kN/cm^2

Axial Stress	Taylor[27]	Sauer[23]	Present	Beam
$\sigma_{11}(0, 0, 420)$	-8.78	-8.77	-8.78	-8.83
$\sigma_{11}(0, 0, 380)$	7.06	7.05	7.06	7.02

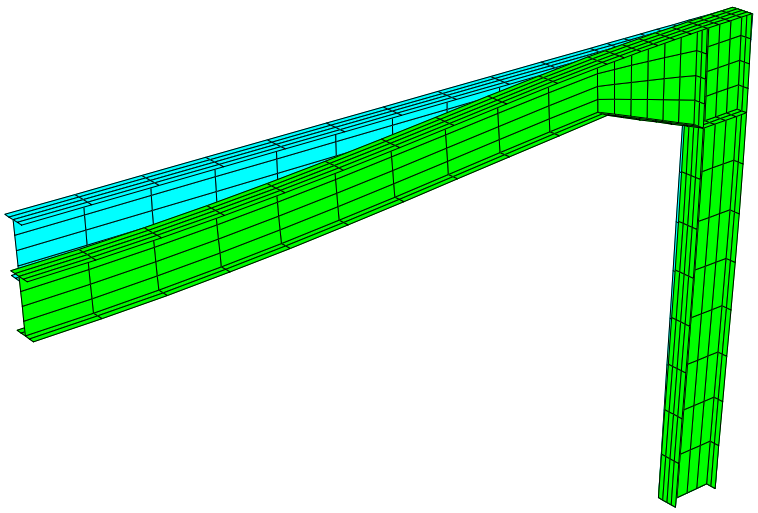

Figure 13: Undeformed and deformed mesh (amplified by a factor 20)

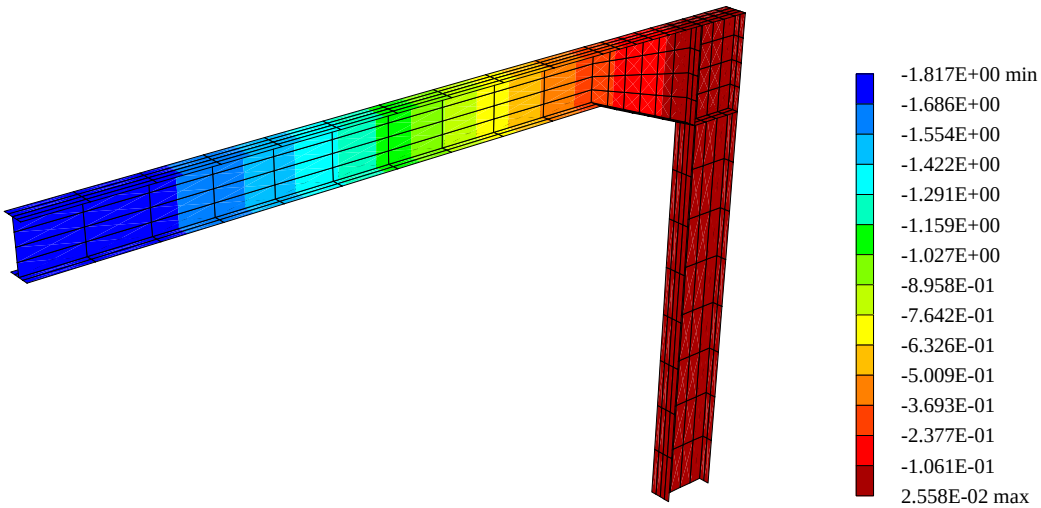

Figure 14: Vertical deflection u_z in cm

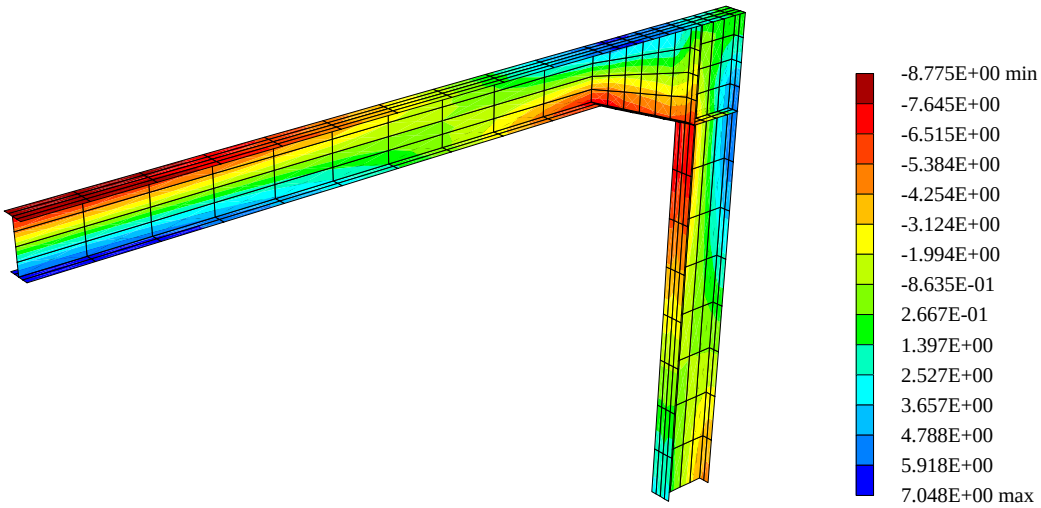

Figure 15: Axial stresses σ_{11} at mid–surfaces in kN/cm^2

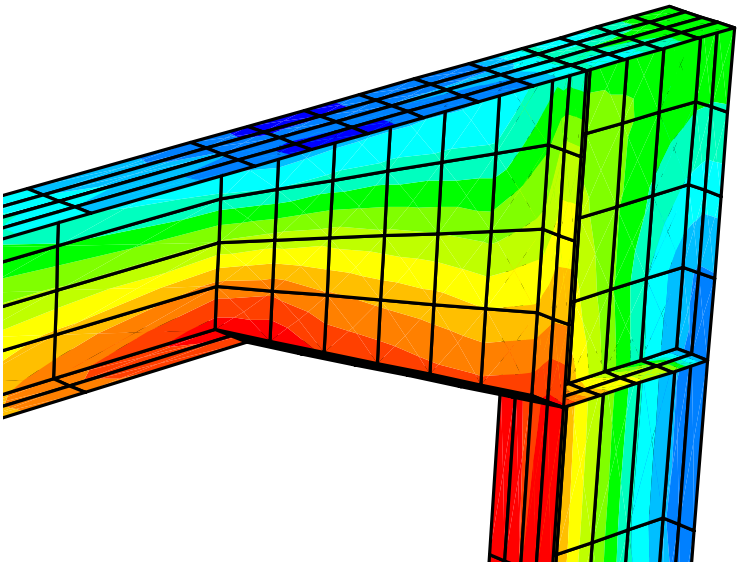

Figure 16: Axial stresses σ_{11} at mid–surfaces in kN/cm^2 in the frame corner

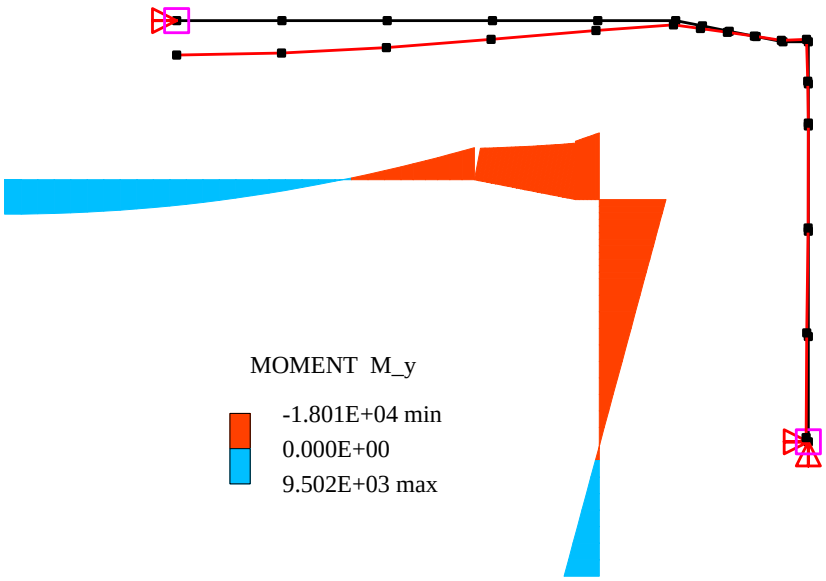

Figure 17: Beam model: undeformed mesh, deformed mesh (amplified by a factor 20) and bending moment

5 Conclusions

The main aspect of the present work is to derive a four–node shell element with explicit representation of the stiffness matrix. The formulation with 5 or 6 nodal degrees of freedom is applicable for shell problems with intersections. The element possesses a correct rank, is free of locking, and can be used for the structural analysis of thin and thick shells. The computed results obtained for various shell problems with positive and negative Gaussian curvature are very satisfactory. Especially the convergence behaviour of the stress resultants is superior to comparable elements. The essential advantage is the fast stiffness computation due to the analytically derived stiffness matrix.

References

[1] Koiter, W.T.: On the nonlinear theory of thin elastic shells, Proc. Kon. Ned. Ak. Wet. B69, 1966, 1-54. 1

[2] Nagdhi, P.M.: The theory of shells, in Handbuch der Physik, Vol. VIa/2, Mechanics of Solids II, C. Truesdell Ed., Springer-Verlag Berlin. 1972 1

[3] Ahmad, S., Irons B.M., Zienkiewicz, O.C.: Analysis of thick and thin shell structures by curved finite elements, Int. J. Num. Meth. Engng., 2, 419–451, 1970. 1

[4] Papadrakakis, M., Samartin, A., Oñate, E. (eds.), IASS-IACM 2000, Proceedings of the Fourth International Colloquium on Computation of Shell & Spatial Structures, Chania, Greece, 2000. 1

[5] Yang, H.T.Y., Saigal, S., Masud, A., Kapania, R.K.: A survey of recent shell finite elements., Int. J. Num. Meth. Engng., 47, 101–127, 2000. 1

[6] Büchter N., Ramm E.: Shell theory versus degeneration–A comparison in large rotation finite element analysis, Int. J. Num. Meth. Engng., 34, 39–59, 1992. 1

[7] Reissner, E.: The effect of transverse shear deformation on the bending of elastic plates, J. Appl. Mech. 12, 69–76, 1945. 1

[8] Mindlin, R.D.: Influence of rotatory inertia and shear flexural motions of isotropic elastic plates, J. Appl. Mech. 18, 31–38, 1951. 1

[9] Liu, K.K., Law S.E., Lam D., Belytschko, T.: Resultant–stress degenerated shell element, Comp. Meth. Appl. Mech. Engrg, 55, 261–300, 1986. 1

[10] Simo, J.C., Fox D.D., Rifai M.S.: On a stress resultant geometrically exact shell model. Part II: The linear theory; Computational aspects, Comp. Meth. Appl. Mech. Engrg, 73, 53–92, 1989. 1, 3.4, 4.3, 1, 4.4, 2, 3, 4

[11] Stanley G.M., Park K.C., Hughes T.J.R., Continuum–Based Resultant Shell Elements, in: Finite Element Methods for Plate and Shell Structures 1: Element Technology, eds. T.J.R. Hughes and E. Hinton, Swansea U.K.: Pineridge Press, 1986. 1

[12] Zienkiewicz, O. C., Taylor, R.L. and Too, J. : Reduced integration techniques in general analysis of plates and shells, Int. J. Num. Meth. Engng., 3, 275–290, 1971. 1

[13] Belytschko, T., Tsay, C.-S.: A stabilization procedure for the quadrilateral plate element with one–point quadrature, Int. J. Num. Meth. Engng., 19, 405–419, 1983. 1, 4.2

[14] Belytschko, T., Lin, J.I., Tsay,C.-S.: Explicit algorithms for the nonlinear dynamics of shells, Comp. Meth. Appl. Mech. Engrg, 42, 225–251, 1984. 1

[15] MacNeal, R. H.: A simple quadrilateral shell element, Comput. Struct., 8, 175–183, 1978. 1

[16] Hughes, T. J. R. and Tezduyar, T. E.: Finite elements based upon Mindlin plate theory, with particular reference to the 4–node bilinear isoparametric element, J. Appl. Mech., 48, 587–595, 1981. 1

[17] MacNeal, R. H.: Derivation of element stiffness matrices by assumed strain distribution, Nuclear Engineering Design, 70, 3–12, 1982. 1

[18] Dvorkin, E., Bathe, K.-J.: A continuum mechanics based four node shell element for general nonlinear analysis, Engineering Computations, 1, 77–88, 1984. 1, 3.2

[19] Bathe, K.J., Dvorkin, E.: A 4–Node Plate bending element based on Mindlin/Reissner theory and a mixed interpolation, Int. J. Num. Meth. Engng., 21, 367–383, 1985. 1, 3.2

[20] Baumann, M., Schweizerhof K., Andrussow S.: An efficient mixed hybrid 4-node shell element with assumed stresses for membrane, bending and shear parts, Engineerung Computations, 11, 69–80 , 1994. 1, 3.4

[21] Sze, K.Y.: An explicit hybrid–stabilized 9–node Lagrangian shell element, Comp. Meth. Appl. Mech. Engrg, 117, 361–379, 1994. 1

[22] Simo, J.C., Rifai, M.S.: A class of mixed assumed strain methods and the method of incompatible modes, Int. J. Num. Meth. Eng., 29, 1595–1638, 1990. 1

[23] Sauer, R.: *Eine einheitliche Finite–Element–Formulierung für Stab– und Schalentragwerke mit endlichen Rotationen*, Bericht 4 (1998), Institut für Baustatik, Universität Karlsruhe (TH). 1, 4.3, 1, 4.4, 2, 3, 4, 5, 6, 7, 8

[24] Belytschko, T., Leviathan, I.: Physical stabilization of the 4–node shell element with one point quadrature, Comp. Meth. Appl. Mech. Engrg, 113, 321–350, 1994. 1

[25] Cardoso, R.P.R., Yoon, J.-W., Grácio, J.J., Barlat, F., César de Sá, J.M.A.: Development of a one point quadrature shell element for nonlinear applications with contact and anisotrpoy, Comp. Meth. Appl. Mech. Engrg, 191, 5177–5206, 2002. 1

[26] Reese, S., Wriggers, P.: A stabilization technique to avoid hourglassing in finite elasticity, Int. J. Num. Meth. Engng., 48, 79–109, 2000. 1

[27] Taylor, R. L.: Finite element analysis of linear shell problems, in: J.R. Whiteman (Ed), The Mathematics of Finite Elements and Applications VI, (MAFELAP 1987), Academic Press Ltd., London, 1988, p. 191–204. 1, 3.1, 3.6, 3.6, 4.3, 1, 4.4, 2, 3, 4, 5, 6, 7, 8

[28] Gruttmann, F., Wagner, W.: A stabilized one–point integrated quadrilateral Reissner–Mindlin plate element, Int. J. Num. Meth. Engng., 61, 2273-2295, 2004. 3.2, 3.5

[29] Pian, T. H. H. and Sumihara, K.: Rational approach for assumed stress finite elements. Int. J. Num. Meth. Eng., 20, 1685-1695, 1984. 3.4

[30] Zienkiewicz, O.C., Taylor, R.L.: The Finite Element Method Vol. 1–3, 5. ed., Butterworth-Heinemann, Oxford, 2000. 3.4, 3.4, 4

[31] Hughes, T.J.R., Liu W.K.: Nonlinear finite element analysis of shells: Part I. Threedimensional shells, Comp. Meth. Appl. Mech. Engrg, 26:331–362, 1981. 3.6

[32] Simo, J.C.: On a stress resultant geometrically exact shell model. Part VII: Shell intersections with 5/6-DOF finite element formulations, Comp. Meth. Appl. Mech. Engrg, 108, 319–339, 1993. 3.6

[33] MacNeal, R.H., Harder R.L.: A proposed standard set of problems to test finite element accuracy, Finite Elements in Analysis and Design, 1, 3–20, 1985. 4.1, 4.3, 4.5

[34] Lee, S. L., Ballesteros, P.: Uniformly loaded rectangular plate supported at corners, Int. J. Mech. Sci., 2, 206–211, 1960. 4.2

[35] Jetteur, P., Improvement of the quadrilateral Jet shell element for a particular class of shell problems, IREM Internal Report 87/1, Ecole Polytechnique Fédérale de Lausanne, 1987. 4.5

[36] Duddeck, H.: Die Biegetheorie der flachen hyperbolischen Paraboloidschale $z = \bar{c}\,xy$, Ing. Archiv, 31, 44–78, 1962. 4.6, 5, 6